JACS
JOURNAL OF THE AMERICAN CHEMICAL SOCIETY

Communication

pubs.acs.org/JACS

Molten *o*-H_3PO_4: A New Electrolyte for the Anodic Synthesis of Self-Organized Oxide Structures – WO_3 Nanochannel Layers and Others

Marco Altomare,[†] Ole Pfoch,[†] Alexei Tighineanu,[†] Robin Kirchgeorg,[†] Kiyoung Lee,[†] Elena Selli,[§] and Patrik Schmuki*[,†,‡]

[†]Department of Materials Science, Institute for Surface Science and Corrosion WW4-LKO, Friedrich-Alexander University, Martensstraße 7, D-91058 Erlangen, Germany

[‡]Chemistry Department, Faculty of Sciences, King Abdulaziz University, 80203 Jeddah, Saudi Arabia Kingdom

[§]Department of Chemistry, University of Milano, Via C. Golgi 19, I-20133 Milan, Italy

Supporting Information

ABSTRACT: We introduce the use of pure molten *ortho*-phosphoric acid (*o*-H_3PO_4) as an electrolyte for self-organizing electrochemistry. This electrolyte allows for the formation of self-organized oxide architectures (one-dimensional nanotubes, nanochannels, nanopores) on metals such as tungsten that up to now were regarded as very difficult to grow self-ordered anodic oxide structures. In this work, we show particularly the fabrication of thick, vertically aligned tungsten oxide nanochannel layers, with pore diameter of ca. 10 nm and illustrate their potential use in some typical applications.

Ever since the work of Masuda et al., which showed that a simple but optimized electrochemical anodization approach can be used to grow in an entirely self-organized manner vertically aligned one-dimensional (1D) structures,[1] electrochemical anodizing has found wide interest for the controlled and defined growth of nanopores and nanotubular oxide arrays.

While Masuda and follow-up work demonstrated that highly ordered porous alumina can be grown on Al in various aqueous acidic solutions, other reports on anodization found fluoride containing solvents (aqueous or organic) capable of forming highly ordered oxide nanotube structures this first on titanium,[2] then on a wide range of metal substrates.[3,4] In parallel, Melody and Habazaki found that hot glycerol electrolytes[5,6] can provide another platform to establish self-organizing electrochemical conditions (leading to ordered oxide nanochannels on various metals).

In the present work we report on a novel class of a fluoride-free electrolyte, based entirely on molten pure phosphoric acid, which enables the formation of highly ordered, high aspect ratio oxide structures on some elements where self-organizing anodization is considered most challenging. Examples are 1D oxide structures formed from W metal and a full range of other oxide/metal systems such as Nb or Al, as illustrated in Figure 1.

In the present work we focus particularly on WO_3, as the synthesis of such defined WO_3 channel structures could not be achieved using other common techniques, such as hydrothermal processes,[7,8] spray pyrolysis,[9] sputtering,[10] and thermal/e-beam evaporation.[11,12]

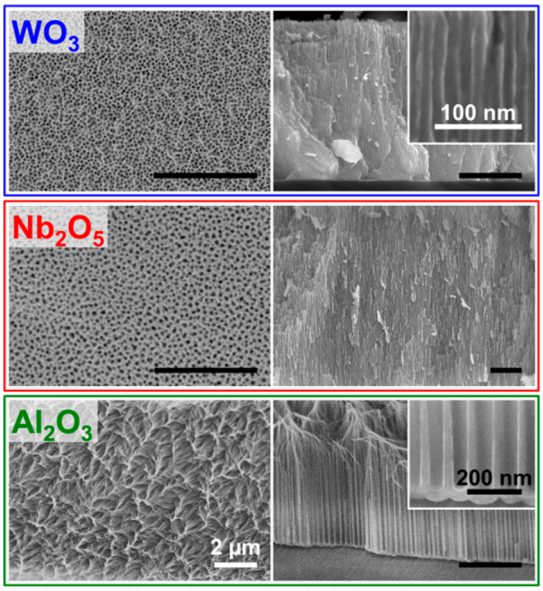

Figure 1. SEM images of different anodic oxide films grown in molten pure *o*-H_3PO_4: WO_3 nanochannel grown on tungsten foil at 5 V and 100 °C; Nb_2O_5 nanochannels grown by anodizing a Nb foil at 10 V and 100 °C; Al_2O_3 nanopores grown by anodizing an Al foil at 40 V and 20 °C.

We first explored anodizing in molten *o*-H_3PO_4 by an extensive screening of various parameters (provided in the Supporting Information). We observed that, namely, voltage, anodization time, temperature, and water content were of high importance (the main results are summarized in Tables S1 and S2). As a result we found the use of pure (nominally water free, i.e., no added water) molten *ortho*-phosphoric acid at 100 °C, in a range of potential of 1−20 V, to be a most suitable range of conditions for achieving self-organizing anodization.

Under these conditions, the diameter of the anodic films can be controlled by varying applied voltage, and the channel-layer thickness by the anodization time. This is illustrated in Figures 2 and 3, which show an optimized anodization approach at 5 V that

Received: February 26, 2015
Published: April 17, 2015

DOI: 10.1021/jacs.5b02104
J. Am. Chem. Soc. 2015, 137, 5646−5649

leads to WO_3 nanochannels with a mean inner diameter of 10 nm (see also Figure S1).

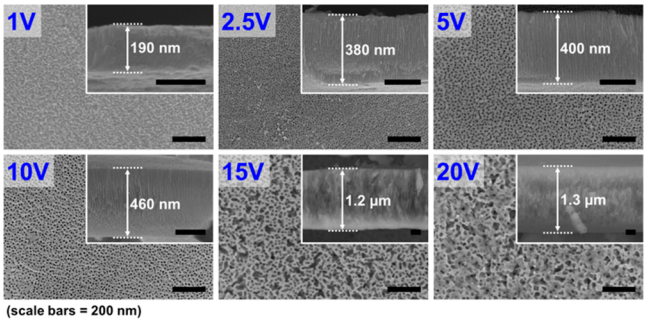

Figure 2. SEM images of WO_3 nanochannel layers fabricated by anodizing W foils in pure molten *o*-H_3PO_4 (100 °C, 1 h) at different voltages (1–20 V).

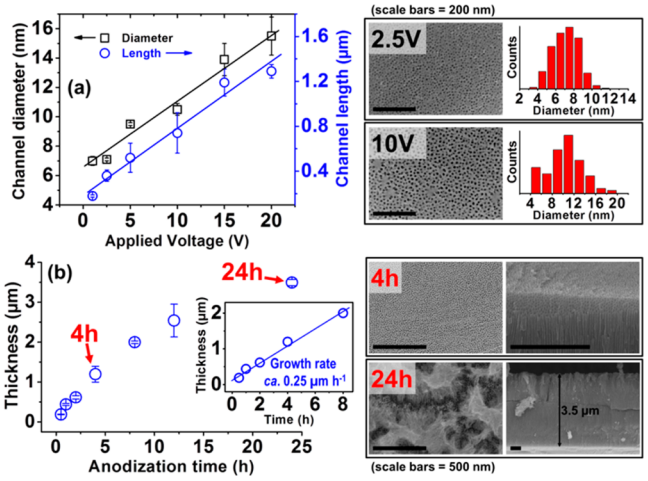

Figure 3. (a) Average inner diameter and length of WO_3 nanochannels grown in molten pure *o*-H_3PO_4 (1 h) at different anodizing voltages (the boxes on the right show top-view SEM images and pore diameter distribution for nanochannels grown at 2.5 and 10 V). (b) Average thickness of WO_3 nanochannel layers grown in molten pure *o*-H_3PO_4 for different anodization times (the boxes on the right show top-view and cross-sectional SEM images of films grown for 4 and 24 h).

Both diameter and length of the nanochannels linearly increase by raising the anodizing voltage from 1 V up to 20 V. Also, for experiments up to 8 h, we found that the layer thickness linearly increased over the anodization time with an average growth rate of ca. 0.25 μm h^{-1} (Figure 3b, inset). Most importantly, these films show over the entire parameter range a morphology consisting of straight nanochannels with top open pores. For longer experiments, the thickening of the WO_3 layers follows a parabolic trend with anodization time, as etching of the outermost part of the film becomes noticeable (Figure 3b).[13]

The electrolyte temperature was found important to establish an ideal equilibrium between field-assisted passivation and oxide dissolution (that is a prerequisite for self-ordering anodization[14−16]); in the case of W an *optimum* is obtained at around 100 °C. At lower temperatures (60 or 80 °C, Figure S2) only a compact oxide or relatively thin porous layers formed, respectively, while ca. 0.5 μm-long nanochannels could be obtained at 120 °C (these showed a considerable etching at the outermost part of the anodic film due to the faster oxide dissolution at elevated temperatures).

In regards to the anodizing voltage, we found an applied potential range of 2.5−10 V to be ideal to form thick and ordered layers. The corresponding current density (J) vs time profiles (Figure S3) indicated that steady state current density values in the range of 0.1−0.6 mA cm^{-2} are required to establish a controlled oxide growth. For lower anodization voltages (1 V), only some tens of nm-thick porous layers were formed (with a current density of only a few μA cm^{-2}). Potentials of 15 V or higher led to significantly less ordered nanochannel layers (Figure 2, in agreement with too high current density values in the range of tens of mA cm^{-2}, as shown in Figure S3).

Another key factor is the water content: this is because, although nominally water-free molten *o*-H_3PO_4 is used, the key oxidant is remnant of water. Noteworthy, pure *o*-H_3PO_4 is sufficiently hygroscopic to maintain a certain water level in the electrolyte. In fact, Karl Fischer analysis (see the Supporting Information for details) demonstrated that the water content of (nominally) pure *o*-H_3PO_4, molten and heated up to 100 °C, is of approximately 1.1% (see Figure S4), i.e., limited water content in the electrolyte is essential to reach a controlled growth of thick and ordered porous films.

To illustrate the importance of the water concentration we performed anodization experiments (under otherwise optimized conditions) during which a relatively little amount of water was added to the electrolyte (to reach a nominal water content of ca. 0.5 vol %) and by growing anodic films in *o*-H_3PO_4-based electrolytes with different initial (nominal) water contents.

As shown in Figure 4, while water additions up to 2 vol % did not affect the film structure, larger amounts of water (e.g., 10 vol %) led to a strong increase of the etching rate (higher solubility of the anodic oxide) and consequently to a disordered porous film. Water effects are also apparent from the J−time profile in Figure

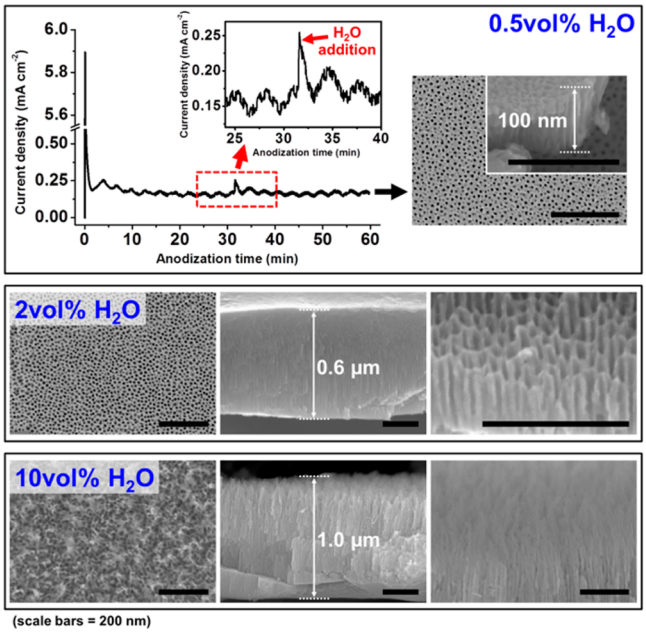

Figure 4. J−time profile of an anodization experiment performed on W foil in optimized conditions (molten *o*-H_3PO_4, 5 V, 100 °C, 1 h) during which after ca. 30 min of anodization 100 μL of DI H_2O were added to the electrolyte (so to reach a "nominal" DI H_2O concentration of ca. 0.5 vol %). On the right, SEM images of the obtained structure; SEM images of WO_3 nanochannel films grown in *o*-H_3PO_4-based electrolytes with initial nominal water content of 2 and 10 vol % (5 V, 100 °C, 1 h).

DOI: 10.1021/jacs.5b02104
J. Am. Chem. Soc. 2015, 137, 5646−5649

4 where a sharp positive spike is observed at the time of water addition. This reflects a sudden acceleration of oxide dissolution. However, in the case of small amounts of added water, the current density typically recovers in a few minutes to a steady state value and the anodization experiment finally leads to a highly ordered structure (Figure 4, SEM images on the right side). These results can be explained by assuming that relatively small amounts of added water can rapidly evaporate from the hot *o*-H_3PO_4 electrolyte, so that the electrolyte reaches at the equilibrium a limited water content.

Typical WO_3 porous films (as those shown in Figures 2−4) were characterized in view of their composition and structure. As-formed anodic films were in every case amorphous, as evident from XRD, HRTEM, and SAED data in Figure 5a,b. The

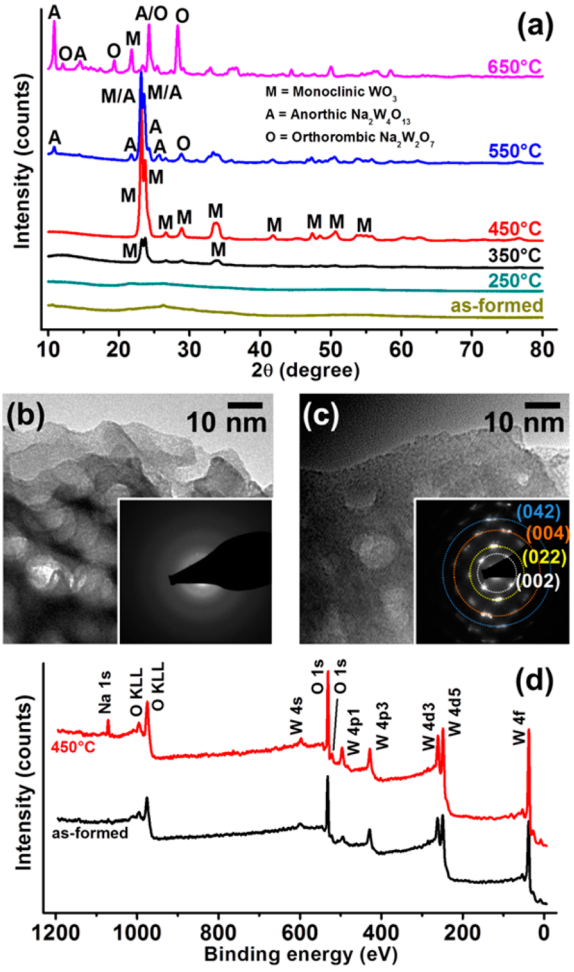

Figure 5. (a) XRD, (b,c) TEM, and (d) XPS characterization of nanochannel layers grown by anodization in pure molten *o*-H_3PO_4 at 5 V and 100 °C. (a) XRD patterns of as-formed and annealed layers (annealing temperature in the 250−650 °C range, air, 1 h); (b,c) HRTEM images and SAED patterns (insets) of (b) as-formed and (c) annealed (450 °C) films; (d) XPS survey spectra of as-formed and annealed films.

conversion into crystalline structures could be obtained by a thermal treatment in air. Crystallization into monoclinic WO_3 could be achieved by annealing at 350 °C (Figure 5a).[17−19] For layers annealed at 450 °C we observed significantly more intense reflections, ascribed to a higher crystallinity. The crystallization of these layers was further confirmed by clearly visible lattice planes of crystalline WO_3 in the HRTEM image (Figure 5c). Also, the SAED pattern showed a 4-fold symmetry with *d* spacing of 3.86, 2.70, 1.93, and 1.69 Å corresponding to the (002), (022), (004), and (042) planes of monoclinic WO_3.[20] Higher temperatures led to significant sintering and collapse of the nanochannels (Figures S5−S7).

XPS analysis of both as-formed and annealed layers confirmed the formation of WO_3 (Figure 5d), with the W $4f_{7/2}$ and W $4f_{5/2}$ peaks centered at 36.71 and 38.91 eV (in line with the literature[21]), and a W/O ratio of ca. 1:3.4. Additionally, XPS analysis revealed the presence of P (ca. 1.1 at %) in both as-formed and annealed films (Figure S8).[22] These results are well in line with those provided by EDX measurements, which revealed P contents of ca. 1.1−1.2 at % (Figure S9), and are thus indicative of the formation of WO_3−PO_4 adsorbates at the interface (a PO_4-terminated surface of the oxide might also be the reason for the relatively large O/W atomic ratio compared to stoichiometric WO_3).

Overall, it can be concluded that the key role of the molten phosphate electrolyte is 2-fold: (i) it provides an environment with controlled and limited water content, and (ii) it provides phosphate ions that protect the WO_3 layer from rapid dissolution. In fact we explored different phosphate sources and found that also other phosphorus-containing acids, namely, hot (nominally pure) pyro- and polyphosphoric acids are also suitable electrolytes for the growth of such ordered porous WO_3 structures (Table S3 and Figure S10).

Because of its electronic and optical properties, WO_3 has received large attention in the last decades in scientific and technological fields:[23] among other applications, it has been investigated as photocatalyst,[24] to fabricate electrodes for electrochromic devices,[25,26] and for photoelectrochemical cells (i.e., water splitting),[27] and it has been intensively studied also for its gas-sensing properties.[13,28−30] In these applications, such a WO_3 nanochannel structure, with its highly defined geometry, can represent a key for obtaining improved performance owing, namely, to advantageous directional charge transfer, enhanced gas diffusion, and ion intercalating geometry, in comparison to devices fabricated from classical powder assemblies.

To illustrate a possible technological application, we fabricated from our WO_3 nanochannel layers H_2 gas-sensors (see the Supporting Information). In comparison to previous literature reports on WO_3-based sensors (Pt- or Pd-decorated) showing reliable detection of H_2 only down to a concentration of ca. 40 ppm at room temperature[31] or down to 5 ppm at 250 °C,[30] our Pt-contacted structures show nearly two-orders (80-times) and one-order of magnitude lower limits of detection, respectively (see Figure S14). Other applications may be especially in the field of catalysis and for fabricating photoelectrochemical devices (photoanodes, Figure S15).

In summary, in the present work we introduced a new anodization approach, based on the use of hot pure phosphoric acid as anodizing electrolytes, to form highly self-organized nanochannel structures of WO_3 and also of various other metal oxides including Al and Nb oxides. We showed that this effect is not only limited to pure hot *ortho*-phosphoric acid but also can be achieved using pyro- and polyphosphoric acids. The functionality and potential technological usefulness of the anodic porous films grown by this method were also briefly illustrated by fabricating highly sensitive H_2 gas-sensors.

DOI: 10.1021/jacs.5b02104
J. Am. Chem. Soc. 2015, 137, 5646−5649

■ ASSOCIATED CONTENT

Supporting Information

Experimental section; preliminary anodization experiments (parameter screening); SEM, XPS, EDX, XRD, and Karl Fischer analysis; H_2-sensors and photoanodes fabrication, and relative gas-sensing and photoelectrochemical water splitting results. This material is available free of charge via the Internet at http://pubs.acs.org.

■ AUTHOR INFORMATION

Corresponding Author

*schmuki@ww.uni-erlangen.de

Notes

The authors declare no competing financial interest.

■ ACKNOWLEDGMENTS

Ulrike Marten-Jahns and Dr. Lei Wang are acknowledged for helping in the evaluation of the diffraction data. Helga Hildebrand and Dr. Anca Mazare are acknowledged for technical help and fruitful discussion on XPS data. Dr. Mirza Mackovic and Florian Niekiel are acknowledged for technical help in TEM analysis and data evaluation. Prof. Dr. Peter Wasserscheid (Institute of Chemical Reaction Engineering, Friedrich-Alexander University) and Marlene Scheuermeyer are acknowledged for technical help with Karl Fischer analysis. The authors would also like to acknowledge the ERC, the DFG, and the Erlangen DFG cluster of excellence EAM for financial support. M.A. and E.S. acknowledge financial support from MIUR through the 2009PASLSN PRIN project.

■ REFERENCES

(1) Masuda, H.; Fukuda, K. *Science* **1995**, *268*, 1466.
(2) Assefpour-Dezfuly, M. *J. Mater. Sci.* **1984**, *19*, 3626.
(3) Roy, P.; Berger, S.; Schmuki, P. *Angew. Chem., Int. Ed.* **2011**, *50*, 2904.
(4) Kowalski, D.; Kim, D.; Schmuki, P. *Nano Today* **2013**, *8*, 235.
(5) Melody, B.; Kinard, T.; Lessner, P. *Electrochem. Solid-State Lett.* **1999**, *1*, 126.
(6) Lu, Q.; Alcalá, G.; Skeldon, P.; Thompson, G.; Graham, M.; Masheder, D.; Shimizu, K.; Habazaki, H. *Electrochim. Acta* **2002**, *48*, 37.
(7) Lakshmi, B.; Patrissi, C.; Martin, C. *Chem. Mater.* **1997**, *20*, 2544.
(8) Yang, P.; Zhao, D.; Margolese, D. *Nature* **1998**, *396*, 152.
(9) Matei Ghimbeu, C.; van Landschoot, R. C.; Schoonman, J.; Lumbreras, M. *Thin Solid Films* **2007**, *515*, 5498.
(10) Sberveglieri, G.; Depero, L.; Groppelli, S.; Nelli, P. *Sens. Actuators, B* **1995**, *26*, 89.
(11) Lee, S.; Cheong, H.; Tracy, C. E. *Electrochim. Acta* **1999**, *44*, 3111.
(12) Antonaia, A.; Addonizio, M.; Minarini, C. *Electrochim. Acta* **2001**, *46*, 2221.
(13) Shaver, P. J. *Appl. Phys. Lett.* **1967**, *11*, 255.
(14) Houser, J. E.; Hebert, K. R. *Nat. Mater.* **2009**, *8*, 415.
(15) Hebert, K. R.; Albu, S. P.; Paramasivam, I.; Schmuki, P. *Nat. Mater.* **2012**, *11*, 162.
(16) Zhou, X.; Nguyen, N. T.; Özkan, S.; Schmuki, P. *Electrochem. Commun.* **2014**, *46*, 157.
(17) Mukherjee, N.; Paulose, M.; Varghese, O. K.; Mor, G. K.; Grimes, C. A. *J. Mater. Res.* **2011**, *18*, 2296.
(18) Tsuchiya, H.; Macak, J. M.; Sieber, I.; Taveira, L.; Ghicov, A.; Sirotna, K.; Schmuki, P. *Electrochem. Commun.* **2005**, *7*, 295.
(19) Berger, S.; Tsuchiya, H.; Ghicov, A.; Schmuki, P. *Appl. Phys. Lett.* **2006**, *88*, 203119.
(20) Loopstra, B. O.; Rietveld, H. M. *Acta Crystallogr., Sect. B: Struct. Crystallogr. Cryst. Chem.* **1969**, *25*, 1420.
(21) Yous, B.; Robin, S.; Donnadieu, A.; Dufour, G.; Maillot, C.; Roulet, H.; Senemaud, C. *Mater. Res. Bull.* **1984**, *19*, 1349.
(22) Bauer, S.; Kleber, S.; Schmuki, P. *Electrochem. Commun.* **2006**, *8*, 1321.
(23) Zheng, H.; Ou, J. Z.; Strano, M. S.; Kaner, R. B.; Mitchell, A.; Kalantar-Zadeh, K. *Adv. Funct. Mater.* **2011**, *21*, 2175.
(24) Abe, R.; Takami, H.; Murakami, N.; Ohtani, B. *J. Am. Chem. Soc.* **2008**, *130*, 7780.
(25) Deb, S. K. *Philos. Mag.* **1973**, *27*, 801.
(26) Ou, J. Z.; Balendhran, S.; Field, M. R.; McCulloch, D. G.; Zoolfakar, A. S.; Rani, R. A.; Zhuiykov, S.; O'Mullane, A. P.; Kalantar-zadeh, K. *Nanoscale* **2012**, *4*, 5980.
(27) Hodes, G.; Cahen, D.; Manassen, J. *Nature* **1976**, *260*, 312.
(28) Xu, Z. *J. Vac. Sci. Technol., A* **1990**, *8*, 3634.
(29) Smith, D. J.; Vatelino, J. F.; Falconer, R. S.; Wittman, E. L. *Sens. Actuators, B* **1993**, *13*, 264.
(30) Mozalev, A.; Calavia, R.; Vázquez, R. M.; Gràcia, I.; Cané, C.; Correig, X.; Vilanova, X.; Gispert-Guirado, F.; Hubálek, J.; Llobet, E. *Int. J. Hydrogen Energy* **2013**, *38*, 8011.
(31) Kukkola, J.; Mäklin, J.; Halonen, N.; Kyllönen, T.; Tóth, G.; Szabó, M.; Shchukarev, A.; Mikkola, J.-P.; Jantunen, H.; Kordás, K. *Sens. Actuators, B* **2011**, *153*, 293.

DOI: 10.1021/jacs.5b02104
J. Am. Chem. Soc. 2015, 137, 5646−5649